Tunable Tunneling Electroresistance in Ferroelectric Tunnel Junctions by Mechanical Loads

Xin Luo, Biao Wang,* and Yue Zheng*

State Key Laboratory of Optoelectronic Materials and Technologies/Institute of Optoelectronic and Functional Composite Materials, Micro-Nano Physics and Mechanics Research Laboratory, School of Physics and Engineering, Sun Yat-Sen University, Guangzhou 510275, China

ABSTRACT Combining nonequilibrium Green function's approach with density functional theory, effects of the applied mechanical loads on polarization, electrostatic potential, and tunneling conductance of a ferroelectric tunneling junction (FTJ) have been investigated. Using the first principle calculations, we show that compressive strains can induce and enhance the polarization in ferroelectric tunnel barriers, and practically achieve ferroelectricity in two unit cell thickness under a −2.2% compressive strain. More importantly, mechanical strains can significantly change the effective electrostatic potential in FTJ and thus control its tunneling conductance, which is defined as giant piezoelectric resistance (GPR) effect. Our calculations indicate that GPR effect is particularly significant near the paraelectric/ferroelectric phase transition, and increases exponentially with the barrier thickness. Furthermore, it is also found that defects of oxygen vacancies and nitrogen doping have little impact on GPR ratio of strained FTJ. Because of its high-sensitivity to external mechanical loads, FTJ with GPR effect should be adequate for applications in agile mechanical sensors, transducers, and other multifunctional devices.

KEYWORDS: ferroelectric tunneling junction · giant piezoelectric resistance · conductance · strain · phase transition

Ferroelectric materials have broad applications in the multifunctional electronic devices, such as transducers, actuators, sensors, and capacitors, *etc.* Of particular interest are nanoscale ferroelectrics because of the increasingly important role they play in the development of ultrahigh density nonvolatile ferroelectric random access memories (FERAMs). Meanwhile the properties of a ferroelectric material in nanoscale, especially the spontaneous polarization and Curie temperature are well-known to depend on many factors, including sample dimensions, external mechanical loads, surface, and electrostatic boundary conditions *etc.* Therefore, nanoscale ferroelectric structures are also a popular target of fundamental investigation.

Recent interest in the concept of ferroelectric tunnel junction (FTJ) begins to expand for reasons of both scientific curiosity and prospects of practical applications. Unlike the traditional dielectric tunnel junctions (DTJ) and magnetic tunnel junctions (MTJ),[1,2] which are constructed with nonpolar dielectric tunnel barriers, FTJ use ferroelectric materials as the tunneling barriers.[3−5] For a long time, it was commonly believed that there is a critical thickness, below which the ferroelectricity or spontaneous polarization in FTJ would be suppressed due to effects of the surface, interface, and depolarization field.[6] On the basis of first principle calculations, Junquera *et al.*[7] predicted that ultrathin single domain $BaTiO_3$ films between conducting $SrRuO_3$ electrodes lose ferroelectricity below the thickness of 6 unit cells (∼26 Å). At the same time, many experimental studies also found that the ferroelectricity can only be retained above some critical thickness of about 1−10 nm.[8−10] In addition, Fong *et al.*[11] and Aguado *et al.*[12] indicated that the formation of domain structures can even stabilize the ferroelectricity in films with a thickness of 2 unit cells, which is also the minimum size with bulk ferroelectric environment. The existence of ferroelectricity in nanoscale FTJ has led to renewed interest in exploring applications of ferroelectrics in the nanoelectronics.[13−15]

The strong coupling of spontaneous polarization and external field is a prominent feature of FTJ. Particularly, spontaneous polarization in the ferroelectric tunnel barriers (FTB) can be switched by external electric field, which results in different charge distribution at electrode/ferroelectric interfaces. Accordingly, the internal electrostatic potential profile across the junction is different. As proposed by Tsymbal *et al.* and Kohlstedt *et al.*,[16−18] the tunneling electroresistance (TER) across ferroelectric barrier can be adjusted significantly in asymmetry FTJ by the reversal of spontaneous polarization. Switchable polarization in FTB adds a new functional property to the junction. Recent experiments[13,19,20] have directly

* Address correspondence to zhengy35@mail.sysu.edu.cn, wangbiao@mail.sysu.edu.cn.

Received for review July 24, 2010 and accepted January 25, 2011.

Published online February 10, 2011
10.1021/nn1031438

detected evidence for ferroelectricity related giant electroresistance (GER) effect in ultrathin asymmetry FTJ, where the electroresistance can vary by over an order of magnitude due to the effect of polarization reversal.

It is also well-known that the properties of ferroelectrics are highly sensitive to the mechanical loads, such as external applied stresses and strains.[21−23] In ferroelectrics, mechanical loads can modify the delicate balance between long-range dipole−dipole electrostatic interactions and short-range repulsive forces. Their subtle competitions are known as the origin of ferroelectric instability.[24] Therefore, both Curie temperature and polarization state will be sensitively depended on the external mechanical loads. The strong strain-polarization coupling can give rise to a variety of interesting physical properties in ferroelectric materials. For example, Vanderbilt *et al.*[25,26] have investigated the effects of in-plane epitaxial strain on the ground-state structure and obtained the misfit-strain temperature phase diagram of $BaTiO_3$ using a first-principles based model Hamiltonian approach. In thin film ferroelectrics, Spaldin *et al.*[27] found that epitaxial strains can greatly enhance the spontaneous polarization, and the epitaxial strain dependence of the polarization varies for different systems due to their different piezoelectric and elastic constants. On the basis of the coupling of spin, optical phonon, and strain, Rabe *et al.*[28,29] have further proposed a design strategy to achieve multiferroic with stable ferroelectric−ferromagnetic ground state. Although the strain effects are investigated in detail in the bulk ferroelectrics and thin film systems, the influences of electrodes are not considered in their studies, thus the electronic transport properties are missing. On the other hand, the electron tunneling through unstrained ferroelectric barriers was studied by Tsymbal *et al.*[30] using first-principles calculations. They found that the polarization of the $BaTiO_3$ barrier can lead to substantial drop in the tunneling conductance. Subsequent *ab initio* studies[31] have predicted that four resistance states exist in multiferroic tunnel junctions, by changing the magnetization alignment of the electrodes and the polarization orientation in FTB. However, in these literatures, the effects of strain on electron tunneling conductance are still not investigated. In view of earlier findings that the mechanical loads can influence the band gap structure and conductance in nanoscale materials,[32−36] the combination of strain engineering and electron transport in FTJ may lead to novel, yet undiscovered electronic-mechanical multifunctional ferroelectric devices.[34−36] For example, Kohlstedt *et al.*[18,37] have described the influence of converse piezoelectric effect on tunneling current in a simplified one-band model. Owing to the limitation of approximation in their model, many mechanisms related to internal atomic displacement cannot be revealed in their studies. Therefore, a microscopic quantum mechanical method is required to elucidate the effect of mechanical loads on FTJ. Nevertheless, to the best of our knowledge, there are still not such first-principle based theoretical studies to investigate the effects of mechanical loads on the conductance of FTJ.

In this work, we perform *ab initio* density functional theory calculations on a traditional FTJ, that is, Pt/$PbTiO_3$/Pt. The polarization, charge distribution, electrostatic potential profile and transmission probability of Pt/$PbTiO_3$/Pt strained FTJ are investigated. Of particular interest is the possibility of strain tunable resistance in the strained FTJ. It is found that the conductance of FTJ can be modulated by the applied mechanical strains, giving rise to a GER-like effect, which is defined as a giant piezoelectric resistance (GPR) effect. Moreover, applying a modest mechanical strain can sufficiently change the Schottky barrier to produce orders of magnitude change in the resistance. The high-sensitivity of the GPR effect shows that strained FTJ will be potentially useful in applications of high-sensitive electro-mechanical systems and provides more degree of freedom in the design of high performance microelectronic devices.

RESULTS AND DISCUSSION

Structural and Ferroelectric Properties. We use density functional theory (DFT) calculations to investigate the ground state structure of FTJ with external mechanical loads. The model of Pt/$PbTiO_3$/Pt junction is schematically illustrated in Figure 1, where an ultrathin (001) oriented $PbTiO_3$ ferroelectric film is sandwiched by two Pt (001) electrodes. Owing to the lack of detailed experimental information for the atomic structure of Pt/$PbTiO_3$ interface, we examined four different interfacial structures to look for the energy favored one. Both PbO- and TiO_2- terminated interfaces are considered in our models, as shown in Figure 1b and 1c. In the four structures, O atoms in PbO and TiO_2 terminations are located at the top and hollow sites of the outmost Pt layer. To find the most stable structure among these models, we calculate their cohesion energy to quantify the energy required to separate an interface into two free surfaces. The cohesion energy is calculated by[38]

$$W_{co} = (E_{Pt} + E_{PbTiO_3} - E_{Pt/PbTiO_3/Pt})/2A \quad (1)$$

where $E_{Pt/PbTiO_3/Pt}$ is the energy of supercell, E_{Pt} and E_{PbTiO_3} are the corresponding energies of the same supercell containing only Pt or $PbTiO_3$ single component slab, and A is the area of interface. The calculated value of cohesion energy and relative bond lengths for the four models are given in Table 1. It is found that the strongest cohesion energy exists in "2" type interfacial structures, that is, the outmost Pt atoms situated above O atoms in the TiO_2-terminated surface. Accordingly, the minimum energy corresponds to a Pt−O bond length of 2.12 Å. Hence, only the FTJ with "2" type Pt/$PbTiO_3$ configuration is considered in the following calculations.

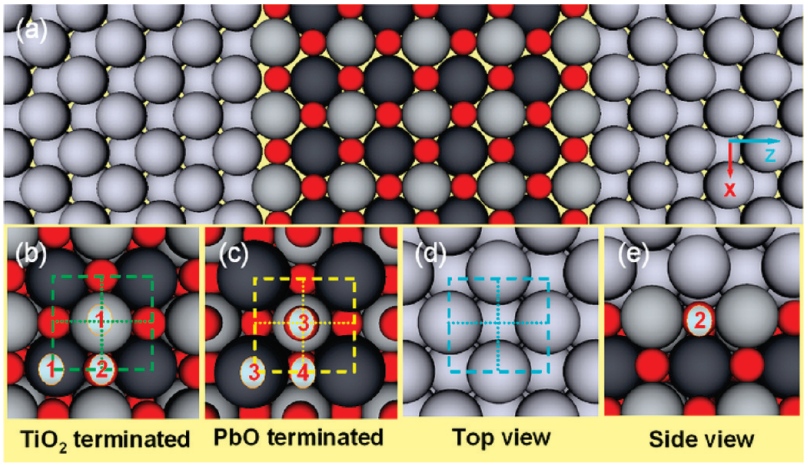

Figure 1. (a) Schematic illustration of the Pt/PbTiO$_3$/Pt system. Four different interface structures are illustrated by "1′′, "2′′, "3′′, and "4" sites for the (b) TiO$_2$- and (c) PbO- terminated interfaces. (d) Top and (e) side views of the most favorite interface structure.

TABLE 1. Calculated Cohesive Energies and Bond Lengths for Different Pt/PbTiO$_3$ Interfaces

interface	W_{co} (J/m^2)	L_{Pt-O} (Å)	L_{Pt-Ti} (Å)	L_{Pt-Pb} (Å)
TiO$_2$ terminated. 1: Ti on top of Pt	1.48	3.22	2.74	
TiO$_2$ terminated. 2: O on top of Pt	4.64	2.12	2.84	
PbO terminated. 3: O on top of Pt	3.76	2.10		2.67
PbO terminated. 4: 4-fold hollow	3.97	3.52		2.97

The basic unit cell of the Pt/PbTiO$_3$/Pt junction can thus has a generic formula [Pt$_{10}$/TiO$_2$-(TiO$_2$−PbO)$_m$/Pt$_{12}$], where m stands for the number of PbTiO$_3$ unit cell. The different thickness of ferroelectric tunnel barriers is monitored by changing m. Accompanied by an in-plane compressive strain, there is an increase in the c/a ratio of PbTiO$_3$, thus enhance the stability of spontaneous polarization in c phase ($P_1 = P_2 = 0$, $P_3 \neq 0$). In principle, when the accumulated elastic energy is very large, the strained thin film will became unstable and defects such as dislocations will appear. As a result, the large strain (*i.e.*, ~4%) is only available in very thin films.[39] For instance, Garcia *et al.*[13,14] have experimentally demonstrated that a large compressive strain of up to −3% can be achieved in the nanoscale ferroelectric thin film with a thickness of 3 nm, indicating that the GPR effect for FTJ is experimentally feasible. In a real FTJ based device, although the junction is under "short-circuit" boundary conditions, the depolarization field is in general nonvanishing if the barrier is in ferroelectric phase. When a symmetric FTJ is in ferroelectric state with the short-circuit boundary conditions, the depolarization field can be approximately given by[34,40−42]

$$E_d = -\frac{P + q_e}{\varepsilon_b} \approx -\frac{1}{\varepsilon_b}\left[1 - \frac{h/\varepsilon_b}{l_{s1}/\varepsilon_{e1} + l_{s2}/\varepsilon_{e2} + h/\varepsilon_b}\right]P \quad (2)$$

where q_e is the surface screening charge density, ε_b is the background dielectric constant of ferroelectrics, h is thickness of the FTB, $\varepsilon_{e1} = \varepsilon_{e2} = \varepsilon_e$ and $l_{s1} = l_{s2} = l_s$ are the dielectric constant and screening length in symmetric electrodes, respectively. It is worth mentioning that the depolarization field E_d in FTB is mainly determined by the polarization P and barrier thickness h. Therefore, we can use the strain to control the depolarization field, charge distribution, and electrostatic potential profile in FTJ due to the electrostrictive coupling between the polarization and mechanical strains.

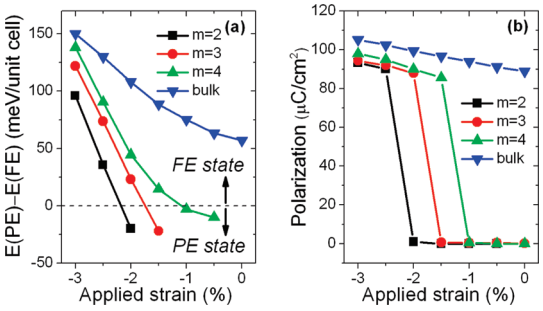

Figure 2. (a) The energy differences between the relaxed ferroelectric/paraelectric barriers in ferroelectric tunneling junction (FTJ) as a function of the applied strain. The thickness of the barrier is change from m = 2 to m = 4 unit cells. (b) Spontaneous polarization of the PbTiO$_3$ barrier as a function of the applied strain.

Based on first principle calculations, Figure 2a shows the energy difference between relaxed paraelectric and ferroelectric states for different thickness. The bulk value in Figure 2a is obtained from a PbTiO$_3$ unit cell imposed the same in-plane strains. It can be seen that the ferroelectricity of FTJ disappears for the thicknesses of m = 2, 3, 4 unit cells without applied strain. These results are consistent with previous studies, where a critical thickness of about 6 unit cells is reported.[43] Furthermore, the ferroelectric state in FTJ began to become stable when larger compressive strain is applied (as shown in Figure 2b). As expected, the polarization in FTB can be induced and enhanced with the increasing compressive strains. For the FTJ

with two unit cell or 1.0 nm barriers, it can switch to stable ferroelectric state in monodomain configuration with a compressive strain of −2.2%. These results indicate that the critical thickness of the FTB is practically tunable in the highly compressive strained FTJ, which opens the possibility of strain control of critical thickness in ferroelectric junctions. Our results are in line with the phenomenological predictions,[37] and recent experimental observation of monodomain with large polarization in ultrathin strained $PbTiO_3$ films.[44] The relationships of applied strains and induced polarizations are given in Figure 2b, it is clear that polarization and critical thickness of FTJ can be controlled by adjusting the applied compressive strains. Because of the restriction of interfacial effect and depolarization field, the polarization in FTJ is smaller than that in bulk ferroelectrics.

Up to now, all the results presented here are performed at zero temperature due to the restriction of DFT ground state calculation. In realistic devices, however, they are running at finite temperature. To get an instructive comparison with experimental observation, much more should be extracted from Figure 2. The Curie temperature T_C for a given strained FTJ can be estimated from the energy difference ΔE between the ferroelectric and paraelectric states.[28] To be specific, we uniformly rescale the energy difference ΔE of unstrained bulk $PbTiO_3$ ferroelectric to its experimental Curie temperature of 765 K. With this energy rescaling method, it is estimated that the Curie temperatures are 470, 990, and 1200 K for the m = 2, 3, and 4 unit cells FTJ under a compressive strain of −2.5%. From Landau mean field theory (see Supporting Information), the polarizations of above strained FTJ are speculated to be 54, 76, and 82 $\mu C/cm^2$ at room temperature, respectively. These predictions can be detected and verified by piezoresponse force microscopy (PFM) in experiment. **Electron Transport Properties in the FTJ.** Presently, the most exciting prospect of FTJ lies in its electronic application. Thus, we calculated the electron transport properties of strained FTJ by using the fully self-consistent nonequilibrium Green's function method combined with first-principles DFT calculation. The tunneling conductance of the above FTJ can be expressed by the classical Büttiker formula[45,46]

$$G = G_0 \sum_{k_\parallel} T(E_F, k_\parallel) \quad (3)$$

where G_0 is the conductance quantum, $T(E_F, \mathbf{k}_\parallel)$ is the transmission coefficient at Fermi energy E_F for a given value of transverse wave vector $\mathbf{k}_\parallel$. Here the transmission coefficient $T(E_F, \mathbf{k}_\parallel)$ can be obtained from the solution of Schrödinger equation for an electron moving in the potential $U(z)$. In general, the overall potential profile $U(z)$ in FTJ can be determined by the properties of two electrodes, ferroelectric tunnel barrier, and the depolarization field E_d.[17,18] In the case of symmetric FTJ, the resulting potential profile $U(z)$ is dominated by the potential barrier height of FTB, which is also strain-dependent. Thus, the conductance of FTJ can be adjusted by applied strains.

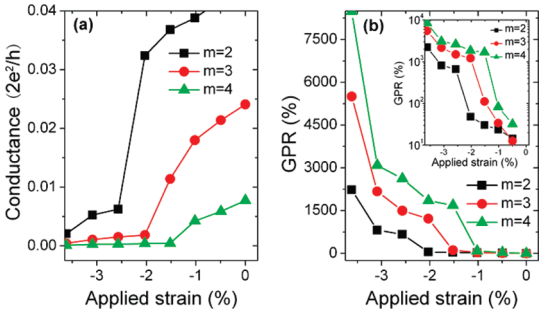

Figure 3. (a) The calculated conductance of the $Pt/PbTiO_3/Pt$ junctions under different applied strain field. (b) Giant piezoelectric resistance (GPR) ratio of the strained FTJ for $PbTiO_3$ films with thicknesses of 1, 1.4, and 1.8 nm. The insert shows the GPR ratio in the logarithmic coordinates.

Figure 3a shows the calculated conductance of $Pt/PbTiO_3/Pt$ junction with respect to a wide range of applied strains. For the m = 4 unit cells FTJ, there is a jump in conductance at the critical compressive strain η_c = −1.1%, below which the barrier switches from paraelectric state to ferroelectric state. A similar behavior is observed in the m = 3,2 unit cells FTJs with a critical compressive strain of −1.7% and −2.2%, respectively. The relative change of resistance R between different strained states is described by giant piezoelectric resistance (GPR) effect. In this work, the GPR ratio is calculated by

$$\mathrm{GPR} = \frac{R_\eta - R_0}{R_0} \quad (4)$$

where R_0 is the tunneling resistance of junction under free bulk condition without any mechanical strain, and R_η is the corresponding value of junction with an applied compressive strain. It is noted that the strain-induced paraelectric/ferroelectric phase transitions play an important role in the electronic transport properties of the junction. Within the strain engineering, we can produce significant large GPR ratios by going through ferroelectric phase transition in a controllable manner. As shown in Figure 3b, the strain modulated GPR ratio for the m = 2 unit cells attains 2230% under a compressive strain of −3.62% (see Supporting Information). The GPR increases dramatically in thicker FTB, reaching about 8500% for the m = 4 (1.8 nm) unit cells strained FTJ. It is predicted that the GPR will further enhance with the increase of FTB thickness and is dominated by the potential barriers.

In the ferroelectric-based devices, the problems such as fatigue, aging, and imprinting have hampered its wider commercialization, and the electrically charge defects are believed to play an important role.[47] Among various defects, oxygen vacancies and nitrogen doping are thought to be the most abundant in

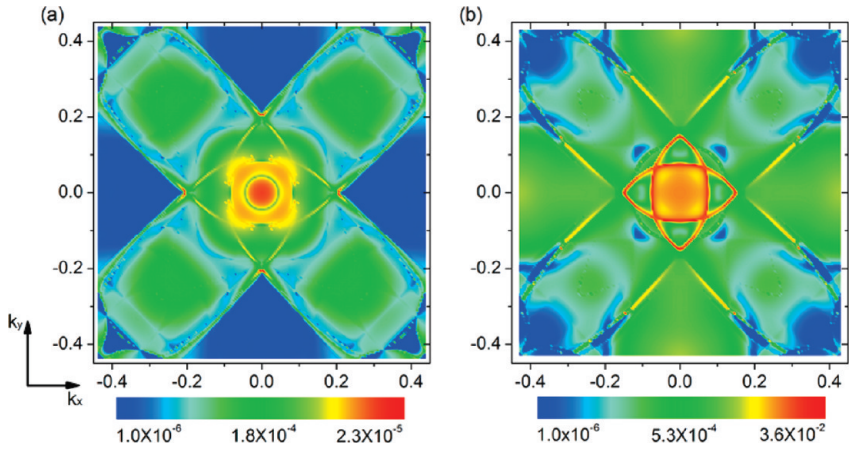

Figure 4. Transmission probability projected in the Brillouin zone at Fermi level for (a) the high compressive strain induced ferroelectric state junction (FTJ_η) and (b) the unstrained paraelectric state junction (FTJ_0).

ferroelectrics. Therefore, we calculated the electronic transport properties of the $m = 4$ unit cells FTJ with the appearance of oxygen vacancies (V_O) or nitrogen doping (N_D) (see Supporting Information). It is clear from Figure S1 that defects in the crystalline lattice generally cause modification of the local fields, making the defect containing junction behave as a perfect junction biased by the electric field. As a result, the paraelectric barrier in unstrained FTJ changed into ferroelectric phase under the defect induced electric field. As indicated in Supporting Information, Table S1, the appearance of V_O defect results in a slightly drop in the GPR ratio, reaching 2310% in the −2.5% compressive FTJ. A similar result is obtained for the N_D defects containing FTJ with a GPR ratio of 1100%. This value of GPR ratio is still large enough for commercial application. Therefore, in such a strained FTJ strategy, the defects are believed to have little influence on the devices performance. While in the high Curie temperature and wide band gap $PbTiO_3$ barrier, the temperature has minor influence on the potential barrier. The merit of manipulating the tunneling resistance by external applied strains is apparent in the future functional devices with high sensitivity and antijamming.

Since the conductance G of $Pt/PbTiO_3/Pt$ junction is determined by transmission probability of the incoming electronic states at the Fermi level E_F, we analyze the $\mathbf{k}_\parallel$ resolved transmission for the $m = 4$ FTJ with different compressive strains. To illustrate the GPR effect, we designate the junction with a high compressive strain $\eta = -2.5\%$ binding as FTJ_η, and the unstrained junction $\eta = 0\%$ is designated as FTJ_0. Figure 4panels a and b show the projection of Fermi level transmission on the $\mathbf{k}_\parallel = (k_x, k_y)$ Brillouin zone for the FTJ_η and FTJ_0, respectively. The high compressive strain induces a ferroelectric phase transition in the barrier, resulting in a ferroelectric state FTB in FTJ_η. Common features seen in the two transmission maps are that contributions to the transmission probability mainly come from areas around the center of Brillouin zone at Γ point ($\mathbf{k}_\parallel = 0$). The transmission probability of FTJ_0 is larger than that of FTJ_η because of the symmetric matching at the electrode/ferroelectric interfaces, as reflected in Figure 4 (note the different scales). The atomic polar displacements that developed along the transport directions of FTJ_η scattered the electron transmission and eliminated some resonant states from the Fermi level.

To gain more insight of the large GPR effect in an atomic scenario, Figure 5 shows the charge density contours of FTJ_η and FTJ_0.[34] The relaxed atomic structures are also given in Figure 5. In FTJ_0, where the FTB is in paraelectric state, the ionic relaxations induce central symmetrical Ti−O rumpling and thus produce interfacial dipoles pointing toward barrier on both sides. Interestingly, the charges in FTJ_0 are distributed symmetrically and extensively. The charges form a connection channel in the barrier, making Pt metallic states penetrate through the barrier, while for the FTJ_η, owning to the elastic effect caused by electrostrictive coupling and lattice strain,[34,37] the depolarization field is suppressed and the spontaneous polarization exists in FTB. As a result, all the Ti ions are shifted away from the center of their respective O cage in FTJ_η. These dipole displacements change the distances between subsurface Ti ions and the outmost Pt electrode by some amounts, which in turn modify the electronic structure dramatically. As is evident from Figure 5, charge density on the interface O and its neighboring Pt are localized and tightly bounded in FTJ_η, the rumplings of Ti−O atoms also contribute to the high decay rate in the barrier. Investigation of structural relaxation also reveals the microscopic interface effect.[18] The Ti−O rumplings in ferroelectric barrier are different at the two interfaces, with the interfacial Pt−O bonding changing from 2.05 to 2.60 Å. These asymmetric displacements modify the microscopic structure of the interfacial region and influenced the barrier potential profiles.

Based on first principle calculations, we have also calculated the effective potential profile to elucidate the effect of applied strain on the FTJ in Figure 6. It is

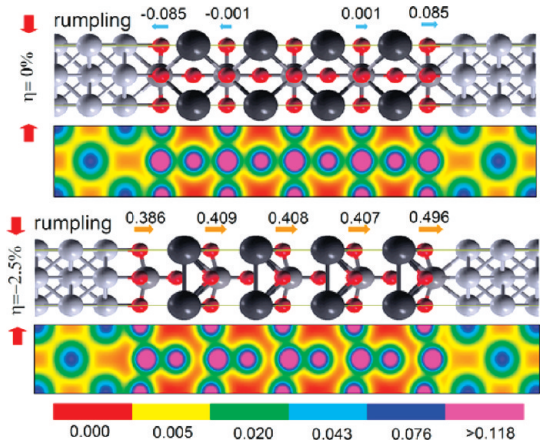

Figure 5. Charge density profiles along the transport direction for the FTJ_0 and FTJ_η. The relaxed atomic structures are shown above the charge density contour, where the arrows show the relative displacement of Ti atoms to the O atoms.

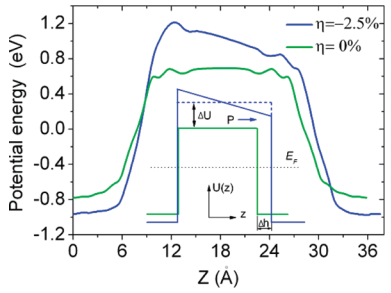

Figure 6. Macroscopic averages of the electrostatic potential energy profile of FTJ_η and FTJ_0. The Fermi level is set to zero as reference energy.

clear that the average potential barrier height of FTJ_η is higher than that of FTJ_0. The mean values of barrier height with respect to the Fermi level of electrode are 1.0 and 0.7 eV for FTJ_η and FTJ_0, respectively. The localized charge density and appearance of microscopic interface effect in FTJ_η greatly enhance the mean value of the electrostatic potential as compared to that in FTJ_0. Indeed, the unscreened polarization charges in FTJ_η give rise to a depolarizing field E_d pointing opposite to the polarization. And the amplitude of E_d can be deduced from the slope of the macroscopic average potential. Owing to the presence of residual depolarizing field E_d, one of the conduction band minimum (CBM) edge is lowered by 0.4 eV. However, the Fermi level is still located inside the band gap of $PbTiO_3$. As indicated in Figure S2, the band gap and Schottky barrier height increase in higher strained FTJs. Another specific feature of the strained FTJ_η is associated with the electrostrictive coupling of strain and polarization. And there will be a step-like increase in the film thickness when the strain induced polarizations appear. The converse piezoelectric effect inherent in ferroelectric material is apparent in FTJ_η, where the barrier is stretched by an amount of Δh due to the electrostrictive effect. In our case, the FTB is elongated by 9.4% in FTJ_η as compared with that in FTJ_0. The combined effect of atomic displacement and electrostrictive coupling results in a large tunneling piezoelectric resistance in FTJ_η.

CONCLUSIONS

We have examined the structural and electronic transport properties of $Pt/PbTiO_3/Pt$ junction under external strain. Through the novel design of constraint FTJ, we have shown that the compressive strains can produce a significant and stable polarization in FTB with thicknesses down to two unit-cells (1 nm). The applied strain could modify the effective potential barrier as well as induce a paraelectric to ferroelectric phase transition in FTJ. Thus, we can control the tunneling conductance of FTJ with strain and produce large GPR effect. Furthermore, it is found that GPR ratio maintained a high sensitivity even if a large amount of V_O and N_D defects appear in the ferroelectric films. The coupling among strain and polarization provides an additional degree of freedom to control the electron transport properties in FTJ. The ability to further tailor the properties in FTJ with the mechanical load offers a tremendously promising future and is still unexplored thoroughly. These results reveal the prospective application of the strain engineering in the design of nanoscale multifunctional devices.

CALCULATION METHODS

Our theoretical calculations are based on density functional theory within the local density approximation (LDA). A plane-wave basis set and projector augmented wave (PAW)[48] potentials as implemented in Vienna ab initio simulation package (VASP)[49] are employed. In the energy calculation, we have used a well converged $8 \times 8 \times 1$ Monkhorst−Pack grid for k-point sampling in the Brillouin zone of the tetragonal supercell, together with a 0.2 eV Gaussian broadening. The plane-wave energy cutoff was set to 480 eV. During the structural relaxation, the ion positions and the out of plane lattice constants were fully relaxed and the configurations were considered as relaxed until the maximum Hellman−Feynman force acting on each ions was less than 0.01 eV/Å. On the basis of these fully relaxed structures, the electronic and ferroelectric properties are calculated. To obtain the ferroelectric properties, we first used the Berry phase approach[50] to calculate the Born effective charge Z^* of the strained bulk $PbTiO_3$, and then the polarizations are calculated by evaluating $P = \Sigma Z^* u$, where u is the ionic displacements relative to their ideal position in paraelectric reference state. The "short-circuit" boundary conditions, equivalent to a metallic contact of top and bottom electrode layers, are imposed by the periodically repeated superlattice structure.[6] To investigate the mechanical loads on the FTJ, we performed strained bulk calculation, where the applied mechanical strain is defined relative to the computed in-plane lattice constants for the relax tetragonal ground state. In our calculation, it is simulated by $\eta = (a_s - a_0)/a_s$,[51] where a_s is the in-plane lattice constant of strained junction and a_0 = 3.866 Å is the relaxed in-plane lattice constant of unstrained bulk $PbTiO_3$. In practice, we start by constraining the in-plane lattice constants of each

superlattice to the fixed a_s, and then relax all the remaining structural parameters.

For the electron transport properties, the conductance and transmission probabilities of the FTJ are explored by the Atomistix ToolKit (ATK),[52] which is based on nonequilibrium Green's function (NEGF) combined with density functional theory (DFT). This method can consider the coupling effects of bulk electrodes through self-energy. The above relaxed structures were used to construct the scattering region, and the periodicity of the supercell in the transport directions was replaced by a matching of two semi-infinite electrodes. As a result, the scattering region consists of the relaxed capacitor structure and two surface layers on the left and right Pt electrodes. The valence electrons are expanded in a numerical atomic-orbital basis set of double ξ plus polarization (DZP) for all atoms except Pt and Pb, for which single ξ plus polarization (SZP) basis are used. Perdew−Zunger local density approximation (LDA) is adopted for exchange-correlation. To get converged results of the conductance, we used a dense k-point mesh of 30 × 30 to sample in the surface two-dimensional Brillouin zone for the two-probe system. All the calculated parameters are tested to result in good convergence.

Acknowledgment. Helpful discussions with M. Q. Cai are gratefully acknowledged. We acknowledge the financial support of the NSFC (Nos. 10732100, 10902128, 50802026, 10972239, 11072271), the Fundamental Research Funds for the Central Universities (No. 3162496), and the Sun Yat-Sen talent cultured project (No. 3126201).

Supporting Information Available: Analysis of the temperature effect on polarization, the influence of the oxygen vacancy and nitrogen doping on the electronic transport properties of FTJ, and the strain dependence of band gap and Schottky barrier height in the central $PbTiO_3$ layer of FTJ. This material is available free of charge *via* the Internet at http://pubs.acs.org.

REFERENCES AND NOTES

1. Baibich, M. N.; Broto, J. M.; Fert, A.; Nguyen Van Dau, F.; Petroff, F.; Eitenne, P.; Creuzet, G.; Friederich, A.; Chazelas, J. Giant Magnetoresistance of (001)Fe/(001)Cr Magnetic Superlattices. *Phys. Rev. Lett.* **1988,** *61*, 2472–2475.
2. Binasch, G.; Grünberg, P.; Saurenbach, F.; Zinn, W. Enhanced Magnetoresistance in Layered Magnetic Structures with Antiferromagnetic Interlayer Exchange. *Phys. Rev. B* **1989,** *39*, 4828–4830.
3. Tsymbal, E. Y.; Kohlstedt, H. Tunneling across a Ferroelectric. *Science* **2006,** *313*, 181–183.
4. Gerra, G.; Tagantsev, A. K.; Setter, N.; Parlinski, K. Ionic Polarizability of Conductive Metal Oxides and Critical Thickness for Ferroelectricity in $BaTiO_3$. *Phys. Rev. Lett.* **2006,** *96*, 107603.
5. Gerra, G.; Tagantsev, A. K.; Setter, N. Ferroelectricity in Asymmetric Metal-Ferroelectric-Metal Heterostructures: A Combined First-Principles−Phenomenological Approach. *Phys. Rev. Lett.* **2007,** *98*, 207601.
6. Ghosez, P.; Junquera, J. First-Principles Modeling of Ferroelectric Oxide Nanostructures. In *Handbook of Theoretical and Computational Nanotechnology*; Rieth, M., Schommers, W., Eds.; American Scientific Publishers: Stevenson Ranch, CA, 2006; Vol. 7, pp 105−254.
7. Junquera, J.; Ghosez, P. Critical Thickness for Ferroelectricity in Perovskite Ultrathin Films. *Nature* **2003,** *422*, 506–509.
8. Tybell, T.; Ahn, C. H.; Triscone, J.-M. Ferroelectricity in Thin Perovskite Films. *Appl. Phys. Lett.* **1999,** *75*, 856–858.
9. Ahn, C. H.; Rabe, K. M.; Triscone, J.-M. Ferroelectricity at the Nanoscale: Local Polarization in Oxide Thin Films and Heterostructures. *Science* **2004,** *303*, 488–491.
10. Dawber, M.; Rabe, K. M.; Scott, J. F. Physics of Thin-Film Ferroelectric Oxides. *Rev. Mod. Phys.* **2005,** *77*, 1083–1130.
11. Fong, D. D.; Stephenson, G. B.; Streiffer, S. K.; Eastman, J. A.; Auciello, O.; Fuoss, P. H.; Thompson, C. Ferroelectricity in Ultrathin Perovskite Films. *Science* **2004,** *304*, 1650–1653.
12. Aguado-Puente, P.; Junquera, J. Ferromagneticlike Closure Domains in Ferroelectric Ultrathin Films: First-Principles Simulations. *Phys. Rev. Lett.* **2008,** *100*, 177601.
13. Garcia, V.; Fusil, S.; Bouzehouane, K.; Enouz-Vedrenne, S.; Mathur, N. D.; Barthélémy, A.; Bibes, M. Giant Tunnel Electroresistance for Non-destructive Readout of Ferroelectric States. *Nature* **2009,** *460*, 81–84.
14. Garcia, V.; Bibes, M.; Bocher, L.; Valencia, S.; Kronast, F.; Crassous, A.; Moya, X.; Enouz-Vedrenne, S.; Gloter, A.; Imboff, D..;; *et al.* Ferroelectric Control of Spin Polarization. *Science* **2010,** *327*, 1106–1110.
15. (a) Zheng, Y.; Woo, C. H. Thermodynamic Modeling of Critical Properties of Ferroelectric Superlattices in Nanoscale. *Appl. Phys. A: Mater. Sci. Process.* **2009,** *97*, 617–626. (b) Woo, C. h.; Zheng, Y. Depolarization in Modeling Nanoscale Ferroelectrics Using Landau Free-Energy Functional. *Appl. Phys. A: Mater. Sci. Process.* **2008,** *91*, 59–63.
16. Rodríguez Contreras, J.; Kohlstedt, H.; Poppe, U.; Waser, R.; Buchal, C.; Pertsev, N. A. Resistive Switching in Metal−Ferroelectric−Metal Junctions. *Appl. Phys. Lett.* **2003,** *83*, 4595–4597.
17. Zhuravlev, M. Ye.; Sabirianov, R. F.; Jaswal, S. S.; Tsymbal, E. Y. Giant Electroresistance in Ferroelectric Tunnel Junctions. *Phys. Rev. Lett.* **2005,** *94*, 246802.
18. Kohlstedt, H.; Pertsev, N. A.; Rodríguez Contreras, J.; Waser, R. Theoretical Current−Voltage Characteristics of Ferroelectric Tunnel Junctions. *Phys. Rev. B* **2005,** *72*, 125341.
19. Maksymovych, P.; Jesse, S.; Yu, P.; Ramesh, R.; Baddorf, A. P.; Kalinin, S. V. Polarization Control of Electron Tunneling into Ferroelectric Surfaces. *Science* **2009,** *324*, 1421–1425.
20. Gruverman, A.; Wu, D.; Lu, H.; Wang, Y.; Jang, H. W.; Folkman, C. M.; Zhuravlev, M. Ye.; Felker, D.; Rzchowski, M.; Eom, C. −B..;; *et al*. Tunneling Electroresistance Effect in Ferroelectric Tunnel Junctions at the Nanoscale. *Nano Lett.* **2009,** *9*, 3539–3543.
21. Choi, K. J.; Biegalski, M.; Li, Y. L.; Sharan, A.; Schubert, J.; Uecker, R.; Reiche, P.; Chen, Y. B.; Pan, X. Q.; Gopalan, V..;; *et al*. Enhancement of Ferroelectricity in Strained $BaTiO_3$ Thin Films. *Science* **2004,** *306*, 1005–1009.
22. Neaton, J. B.; Rabe, K. M. Theory of Polarization Enhancement in Epitaxial $BaTiO_3/SrTiO_3$ Superlattices. *Appl. Phys. Lett.* **2003,** *82*, 1586–1588.
23. Wang, Z. L.; Song, J. H. Piezoelectric Nanogenerators Based on Zinc Oxide Nanowire Arrays. *Science* **2006,** *312*, 242–246.
24. Cochran, W. Crystal Stability and the Theory of Ferroelectricity. *Adv. Phys.* **1960,** *9*, 387–423.
25. Diéguez, O.; Tinte, S.; Antons, A.; Bungaro, C.; Neaton, J. B.; Rabe, K. M.; Vanderbilt, D. *Ab Initio* Study of the Phase Diagram of Epitaxial $BaTiO_3$. *Phys. Rev. B* **2004,** *69*, 212101.
26. Diéguez, O.; Rabe, K. M.; Vanderbilt, D. First-Principles Study of Epitaxial Strain in Perovskites. *Phys. Rev. B* **2005,** *72*, 144101.
27. Ederer, C.; Spaldin, N. A. Effect of Epitaxial Strain on the Spontaneous Polarization of Thin Film Ferroelectrics. *Phys. Rev. Lett.* **2005,** *95*, 257601.
28. Lee, J. H; Rabe, K. M. Epitaxial-Strain-Induced Multiferroicity in $SrMnO_3$ from First Principles. *Phys. Rev. Lett.* **2010,** *104*, 207204.
29. Fennie, C. J.; Rabe, K. M. Magnetic and Electric Phase Control in Epitaxial $EuTiO_3$ from First Principles. *Phys. Rev. Lett.* **2006,** *97*, 267602.
30. Velev, J. P.; Duan, C. G.; Belashchenko, K. D.; Jaswal, S. S.; Tsymbal, E. Y. Effect of Ferroelectricity on Electron Transport in $Pt/BaTiO_3/Pt$ Tunnel Junctions. *Phys. Rev. Lett.* **2007,** *98*, 137201.
31. Velev, J. P.; Duan, C. G.; Burton, J. D.; Smogunov, A.; Niranjan, M. K.; Tosatti, E.; Jaswal, S. S.; Tsymbal, E. Y. Magnetic Tunnel Junctions with Ferroelectric Barriers: Prediction of Four Resistance States from First Principles. *Nano lett.* **2009,** *9*, 427–432.
32. Quek, S. Y.; Kamenetska, M.; Steigerwald, M. L.; Choi, H. J.; Louie, S. G.; Hybertsen, M. S.; Neaton, J. B.; Venkataraman, L. Mechanically Controlled Binary Conductance Switching of a Single-Molecule Junction. *Nat. Nanotechnol.* **2009,** *4*, 230–234.

33. Quek, S. Y.; Choi, H. J.; Louie, S. G.; Neaton, J. B. Length Dependence of Conductance in Aromatic Single-Molecule Junctions. *Nano Lett.* **2009,** *9*, 3949–3953.
34. Zheng, Y.; Woo, C. H. Giant Piezoelectric Resistance in Ferroelectric Tunnel Junctions. *Nanotechnology* **2009,** *20*, 075401.
35. Wu., Z. G; Neaton, J. B.; Grossman, J. C. Charge Separation *via* Strain in Silicon Nanowires. *Nano Lett.* **2009,** *9*, 2418–2422.
36. Wang, Z. Y.; Hu, J.; Suryavanshi, A. P.; Yum, K.; Yu, M. F. Voltage Generation from Individual $BaTiO_3$ Nanowires under Periodic Tensile Mechanical Load. *Nano Lett.* **2007,** *7*, 2966–2969.
37. Pertsev, N. A.; Kohlstedt, H. Elastic Stabilization of a Single-Domain Ferroelectric State in Nanoscale Capacitors and Tunnel Junctions. *Phys. Rev. Lett.* **2007,** *98*, 257603.
38. Oleinik, I. I.; Tsymbal, E. Y.; Pettifor, D. G. Atomic and Electronic Structure of Co/$SrTiO_3$/Co Magnetic Tunnel Junctions. *Phys. Rev. B* **2001,** *65*, 020401.
39. Zheng, Y.; Wang, B.; Woo, C. H. Critical Thickness for Dislocation Generation During Ferroelectric Transition in Thin Film on a Compliant Substrate. *Appl. Phys. Lett.* **2006,** *89*, 083115.
40. Mehta, R. R.; Silverman, B. D.; Jacobs., J. T. Depolarization Fields in Thin Ferroelectric Films. *J. Appl. Phys.* **1973,** *44*, 3379–3385.
41. Tagantsev, A. K.; Gerra, G.; Setter, N. Short-Range and Long-Range Contributions to the Size Effect in Metal−Ferroelectric−Metal Heterostructures. *Phys. Rev. B* **2008,** *77*, 174111.
42. Zheng, Y.; Cai, M. Q.; Woo, C. H. Critical Properties of Symmetric Nanoscale Metal−Ferroelectric−Metal Capacitors. *Acta. Mater.* **2010,** *58*, 3050–3058.
43. Junquera, J.; Ghosez, P. First-Principles Study of Ferroelectric Oxide Epitaxial Thin Films and Superlattices: Role of the Mechanical and Electrical Boundary Conditions. *J. Comput. Theor. Nanosci.* **2008,** *5*, 2071–2088.
44. Fong, D. D.; Kolpak, A. M.; Eastman, J. A.; Streiffer, S. K.; Fuoss, P. H.; Stephenson, G. B.; Thompson, C.; Kim, D. M.; Choi, K. J.; Eom, C. B..;; *et al*.Stabilization of Monodomain Polarization in Ultrathin $PbTiO_3$ Films. *Phys. Rev. Lett.* **2006,** *96*, 127601.
45. Büttiker, M. Four-Terminal Phase-Coherent Conductance. *Phys. Rev. Lett.* **1986,** *57*, 1761–1764.
46. Luo, X.; Wang, B.; Zheng, Y. Microscopic Mechanism of Leakage Currents in Silica Junctions. *J. Appl. Phys.* **2009,** *106*, 073711.
47. Raymond, M. V.; Smyth, D. M. Defects and Charge Transport in Perovskite Ferroelectrics. *J. Phys. Chem. Solid.* **1996,** *57*, 1507–1511.
48. Blöchl, P. E. Projector Augmented-Wave Method. *Phys. Rev. B* **1994,** *50*, 17953–17979.
49. Kresse, G.; Furthmüller, J. Efficiency of *ab-Initio* Total Energy Calculations for Metals and Semiconductors Using a Plane-Wave Basis Set. *J. Comput. Mater. Sci.* **1996,** *6*, 15–50.
50. Vanderbilt, D.; King-Smith, R. D. Electric Polarization as a Bulk Quantity and Its Relation to Surface Charge. *Phys. Rev. B* **1993,** *48*, 4442–4455.
51. Pertsev, N. A.; Zembilgotov, A. G.; Tagantsev, A. K. Effect of Mechanical Boundary Conditions on Phase Diagrams of Epitaxial Ferroelectric Thin Films. *Phys. Rev. Lett.* **1998,** *80*, 1988–1991.
52. Brandbyge, M.; Mozos, J.; Ordejón, P.; Taylor, J.; Stokbro, K. Density-Functional Method for Nonequilibrium Electron Transport. *Phys. Rev. B* **2002,** *65*, 165401.